

Numerical Simulation of Titanium Production  
in the Plasma Quench Reactor

Ray A. Berry and Randall A. LaViolette  
Idaho National Engineering Laboratory  
P.O. Box 1625  
Idaho Falls, Idaho 83415-2210

Robert McGraw  
Brookhaven National Laboratory  
Upton, New York

Abstract

A new and general method for modeling the nucleation of condensates in the steady-state supersonic nozzle flow generated in a plasma quench reactor (PQR). The method enables us to calculate the nucleation rates and the particle-size distribution along any streamline in the flow, without invoking the usual coarse-graining and truncation approximations for the particle-size distribution. We apply the method to titanium condensing in a model argon flow field. The method is directly applicable to simulation of condensation of other metals in other gas flows. We identify the regions in the nozzle of maximum nucleation rate, and show that for the same nucleation rate different particle-size distributions can develop in different regions of the nozzle.

## Introduction

Growing interest has been shown in recent years in the generation of materials with ultrafine microstructure (grain structure between 5 and 100 nanometers) with the expectation that these materials will have properties superior to their coarse-grain counterparts. The unique properties of nanophase materials may lead to new and unusual applications in science and engineering. One method by which nanoclusters can be synthesized is the condensation of nanoclusters from the gas phase, e.g. condensation of metal (or ceramic) vapors in a low pressure, isentropically expanding inert gas [1].

A hybrid version of this process has been developed at the INEL in which a high temperature plasma source is utilized to crack an inflowing stream of appropriate constituents into a reaction chamber. The cracked materials are passed rapidly through a converging-diverging nozzle. As the substance is expanded and cooled, the vapor becomes saturated; then it is supersaturated, during which condensation begins. This process occurs at a rate sufficiently rapid to minimize back reactions. The device has been termed the Plasma Quench Reactor or PQR. The PQR has demonstrated the ability to make nanostructure titanium and ceramic powders as a potentially low cost process. In addition to titanium, nanocrystalline aluminum, vanadium, titanium/vanadium alloy, ceramic titanium carbide, and titanium nitride have been produced using this process. An active area of research is devoted to scaling up this process to provide, for example, titanium powder for the manufacture of auto engine parts and bone and teeth replacements as well as other light weight metal and advanced material products. The small uniform size of the powder makes it suitable for the manufacture of low cost metal matrix composites.

A critical problem with this, as well as other plasma systems, is incomplete mixing of the injected reactants with the plasma. Since residence times are very short in the vapor phase plasma reactors, rapid mixing is required to assure reaction completion.

Designing the reaction chambers and the nozzles for correct mixing, expansion rates, nucleation rates, and condensation and particle growth rates, is nowhere near optimal with current designs. In fact, for some PQR systems, adequate understanding of the pertinent physical processes is even lacking. The objective of this research was to model these plasma quench reactors with computational fluid dynamic techniques coupled with nucleation and condensation growth methods to demonstrate that the technique is useful to (1) gain a better understanding of what physical processes really are occurring in these reactor/nozzle systems, and (2) to guide the design of PQR's toward a more optimal configuration from which scale-up would be deemed feasible.

Here we consider only the problem of the condensation of metals in the nozzle of a model plasma quench reactor that follows the scenario above. We specifically ask the questions: (1) What are the nucleation rates in the flow, and (2) what is the size distribution of the primary particles?

To answer these questions, we combine a high temperature, computational fluid dynamics (CFD) description of the axisymmetric flow of argon gas in a model PQR nozzle, as shown in Figure 1, with a new application of the method of moments for homogeneous nucleation in flow. We consider here the condensation of the refractory metal titanium in the same reactor. In the calculations we treat the metal as a pure vaporized tracer in the argon flow, as though it had already been cracked and mixed uniformly into the reactor flow field, and we assume its condensation leaves the flow undisturbed (one-way coupling). We assume

the former assumption to be reasonable in view of the high temperatures found in the plasma portion of the flow, and the latter to be reasonable in view of the small size and concentration of the particles obtained. We also assume that the metal is entrained along one of the streamlines of the steady flow, the selection of which is determined by the point of injection. This assumption is reasonable in view of the very low mixing between streamlines due to the high viscosity of the gas at high temperatures. The evolution of nucleation and growth on the substantially independent streamlines generated by the flow as provided by the CFD analysis. The one-way coupling assumes, therefore, that the flow parameters along the streamlines dictate the nucleation and growth but that the nucleation and growth have no influence on the flow. Further details of this numerical simulation procedure can be found in [2].

The following section provides a description of the CFD techniques utilized. Then a short development of the nucleation theory is given. Results are then presented, along with some brief discussion, for the application of this technique to the model problem, and conclusion are drawn.

### Computational Fluid Dynamic Technique

The nozzle flow of hot argon gas was described with the Reynolds-averaged Navier-Stokes equations. In integral form, employing summation convention, these equations are

$$\frac{\partial}{\partial t} \int_{Vol} U dV + \int_S \vec{P} \cdot \vec{n} dS = 0 \quad (1)$$

where

$$\vec{P} = F_1 \vec{i} + F_2 \vec{j} + F_3 \vec{k}$$

and

$$U = \begin{bmatrix} \rho \\ \rho u_1 \\ \rho u_2 \\ \rho u_3 \\ E \end{bmatrix}, \quad F_i = \begin{bmatrix} \rho u_i \\ \rho u_i u_i + p \delta_{11} - \tau_{11} \\ \rho u_i u_2 + p \delta_{21} - \tau_{12} \\ \rho u_i u_3 + p \delta_{31} - \tau_{13} \\ (E+p)u_i - u_j \tau_{ij} + q_i \end{bmatrix},$$

and  $\int_S$  indicates a surface integral with unit normal  $\vec{n}$  and  $\int_{Vol}$  indicates a volume integral. Also,  $p$  is the pressure,  $E = \rho(e + u_i u_i / 2)$  is the total energy per unit volume,  $e$  is the internal energy per unit mass, the  $\tau_{ij}$  are the full viscous shear stresses, and  $q_i$  is the total heat transfer rate.

The conservative form of the Navier-Stokes equations are solved using a time-marching (to steady state) finite volume method. Applying the integral conservation equations to each finite volume identified by indices  $i, j, k$

$$\frac{d}{dt} (U_{ijk} Vol_{ijk}) = -(D_i \vec{P} \cdot \vec{S} + D_j \vec{P} \cdot \vec{S} + D_k \vec{P} \cdot \vec{S}) \quad (2)$$

where  $U_{ijk}$  is the mean value of  $U$  in the cell  $ijk$  and  $D_j \vec{P} \cdot \vec{S}$  (for example) represents the difference of the fluxes through opposing  $j$ -faces of the volume.

Inviscid fluxes are calculated at finite volume surfaces using the second-order upwind-

biased flux-splitting scheme of Harten and Yee [3], which in turn is based on the flux-difference splitting method of Roe [4]. Flux limiting is incorporated in order to avoid nonphysical oscillations. The viscous fluxes are calculated at the volume faces with standard second-order central differences. These CFD simulations employ an implicit time differencing scheme with a lower-upper-symmetrical-Gauss-Seidel (LU-SGS) algorithm [5] which is a robust and efficient relaxation procedure for steady state flow fields. The calculations were carried out with the above techniques as embodied in the INCA Code [6].

The fluid dynamics calculations track the flow field parameters  $T$ ,  $u_s$ , and  $\rho$  along each streamline of the nozzle flow for input to the nucleations equations (i.e. Equation (5)).

#### Nucleation Theory of Condensation in a Flow

Here, the method of moments description of nucleation in a continuously stirred tank reactor developed by McGraw and Saunders [7] is extended to the problem of nucleation in a nozzle flow. The growth and evaporation of nucleating particles is described by the system of coupled differential equations [8]

$$\frac{\partial \rho_n}{\partial t} = \Omega_{n-1,n} - \Omega_{n,n+1}, \quad (3)$$

where  $\rho_n$  is the particle-size distribution, i.e. the number density of the particles of size  $n$ , and  $\Omega_{m,n}(\rho_1, \rho_m, \rho_n)$  is the net rate at which a particle of size  $m$  becomes a particle of size  $n$ .

Here we exploit an approach to the description of aerosol nucleation and growth dynamics known as the method of moments [9]. In the moment method, the large number of equations for  $\rho_n$  are replaced by a few equations for the moments of the size distribution, the  $k^{\text{th}}$  moment  $m_k$  being defined by

$$m_k \equiv \sum_{n=1}^{\infty} n^{k/3} \rho_n. \quad (4)$$

For the case of free molecular growth, i.e. particle radius less than the mean free path of the carrier gas, Eqn. (3) can be contracted exactly into a closed system of only four coupled nonlinear equations, without any truncation or coarse-graining of the particle size distribution. In order to adapt the moment equations to nucleation in a steady-state flow we transform the time dependence of the moments into a path dependence. These moment equations for the particle distribution are [7]

$$\begin{aligned} \frac{\partial m_0}{\partial s} &= \frac{m_0}{\rho} \frac{\partial \rho}{\partial s} + \frac{J(\rho_1)}{u_s}, \\ \frac{\partial m_k}{\partial s} &= \frac{m_k}{\rho} \frac{\partial \rho}{\partial s} + \frac{k}{3} \frac{m_{k-1}}{u_s \tau} \frac{(S-1)}{S}, \quad k \geq 1, \\ \frac{\partial \rho_1}{\partial s} &= \frac{\rho_1}{\rho} \frac{\partial \rho}{\partial s} - \frac{m_2}{u_s \tau} \frac{(S-1)}{S}, \end{aligned} \quad (5)$$

where  $J$  is the nucleation rate,  $S$  is the monomer supersaturation ratio,  $\tau$  is the time between monomer collisions,  $\rho$  is the carrier fluid density,  $s$  is the length along a selected one-dimensional streamline of the flow, and  $u_s$  is the velocity at  $s$  along the streamline. The supersaturation is defined by  $S \equiv \rho_1 / \rho_1^{\text{eq}}$ , where the equilibrium concentration  $\rho_1^{\text{eq}}$  is determined from the condensate vapor pressure and ideal-gas equation of state. The kinetic theory of gases gives  $\tau$  through

$$\tau^{-1} = \sqrt{\frac{k_B T}{2\pi m_1}} s_1 \rho_1 \quad (6)$$

where  $k_B$  is the Boltzmann constant,  $s_1$  is the monomer surface area, and  $m_1$  is the monomer mass. The extra factor of  $(S-1)/S$  in Eqn. (5) is included here to describe the effect of particle evaporation in the growth stages. Closure is achieved with only four equations ( $k \leq 2$  above) because the equation for the monomer involves  $m_2$  but no higher moments. However, the sequence is readily continued for tracking higher-order moments of the particle size distribution if these are desired because the time derivative of  $m_k$  depends only on  $m_k$  and  $m_{k-1}$ .

We employ the classical theory due to Becker, Doring, and Zeldovich for nucleation rates  $J$  as expressed in corresponding states form [10]

$$J(\rho_1) = \frac{\Gamma \rho_1^2 2^{1/6}}{\tau} \sqrt{\frac{\Theta}{6\pi}} \exp\left[-\frac{\Theta^3}{(\ln S)^2}\right]. \quad (7)$$

The dimensionless corresponding-states parameter  $\Theta$  is defined by

$$\Theta = \frac{\sigma}{k_B T} \left[ \frac{16\pi v_1^2}{3} \right]^{1/3}, \quad (8)$$

where  $T$  is the absolute temperature,  $v_1$  is the monomer volume, and  $\sigma$  is the condensed phase surface tension. To relate to more modern theories for  $J$ , the replacement factor  $\Gamma$  is included in Eqn. (7). For example, in the Reiss-Katz-Cohen theory,  $\Gamma$  may be as large as  $10^6$  [11]. We retain the classical choice of  $\Gamma = 1$  in our applications because we see little difference between the results of the two theories, although in other applications the choice of  $\Gamma$  might become important.

Frequently one is interested only in integrated properties of an aerosol distribution that can be approximated directly from the lower-order moments of the size distribution without requiring the distribution itself. Here we are interested in examining the distribution itself. We utilize a maximum entropy inversion algorithm to furnish the unique distribution function having the least bias (maximum entropy) subject to the constraints that the known moments are exactly reproduced [12].

The connection between the flow field simulation described above and Eqn. (5) for the nucleation rate and particle-size moments is made explicit with the fluid dynamic calculations tracking the flow field parameters  $T$ ,  $u$ , and  $\rho$  along each streamline of the nozzle flow for input to Eqn. (5). Thus the time between monomer collisions,  $\tau$ , and the nucleation rate  $J$  each depends on the flow field parameters  $T$  and  $\rho$ , through Eqs. (6)-(8). Eqn. (5) are solved along each streamline given by the flow field simulation with an adaptive Runge-Kutta algorithm [13].

### Results and Discussion

The top half of our axisymmetric nozzle through which hot argon gas flows is shown in Figure 1. The half nozzle was simulated with  $129 \times 39$  volumes in the axial and radial directions, respectively. We employed the Baldwin-Lomax turbulence model [14] with a Blottner-type temperature-dependent viscosity formula and a no-slip boundary condition at the wall. We assumed that the nozzle wall was isothermal at a temperature of 1000 K. Our inlet

conditions were specified by a stagnation pressure of 413.5 kPa and a stagnation temperature of 9000 K.

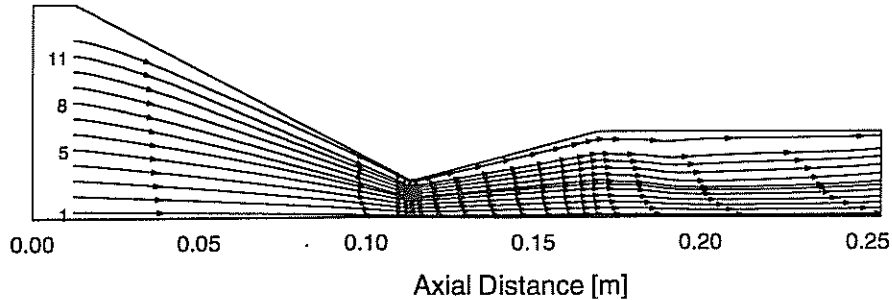


Figure 1. Axisymmetric PQR nozzle and twelve flow streamlines. Arrowheads are spaced at equal time intervals.

The twelve flow streamlines along which nucleation calculations were performed are also shown in Figure 1, the arrow heads along the streamlines being placed at equal time intervals. Figure 2 shows the steady state spatial distribution of the temperature, density, and mach number within the gas flow field.

Figure 3 shows the spatial distribution through the flow field of the (log of) nucleation rate (along streamlines), the (log of) particle density, and the (percent) fraction of titanium vapor which is condensed for an inlet flow stream which has a mole fraction of 0.01 titanium. The latter two plots of this figure have been interpolated from the streamline data to fill the flow region for ease of viewing. We see that the nucleation rate is highest nearer the wall, downstream of the throat. The particle densities are generally highest on the streamlines which had the highest nucleation rates, downstream from where that high nucleation rate occurred. Examination of the outlet plane of the nozzle shows that percentage of titanium vapor which is condensed varies considerably from nearly no condensation near the center line to 100% condensation in the outer third (radially) of the nozzle. Any correspondence between the condensation results of Figure 3 and the gas temperatures and densities of Figure 2 is not readily apparent, emphasizing the importance of numerical simulation to capture these nonlinear effects.

Figure 4 shows the normalized particle size distributions for three different streamlines for the 0.01 mole fraction inlet case. We see that for streamlines nearer the nozzle centerline (streamline 5) the particles have a larger peak size and a narrower distribution while streamlines nearer the wall (streamline 11) have smaller peak sizes with a broader distribution. Finally, in Figure 5 we compare the normalized particle size distribution along the same streamline( 5) resulting from two different inlet flow titanium concentrations, 0.01 and 0.02 mole fraction. We see that by increasing the inlet titanium concentration the particle peak size tends to be reduce and the size distribution is widened.

### Conclusions

The technique we have described and applied for analyzing the nucleation and growth kinetics of titanium powders from the vapor state shows that the complicated, nonlinear

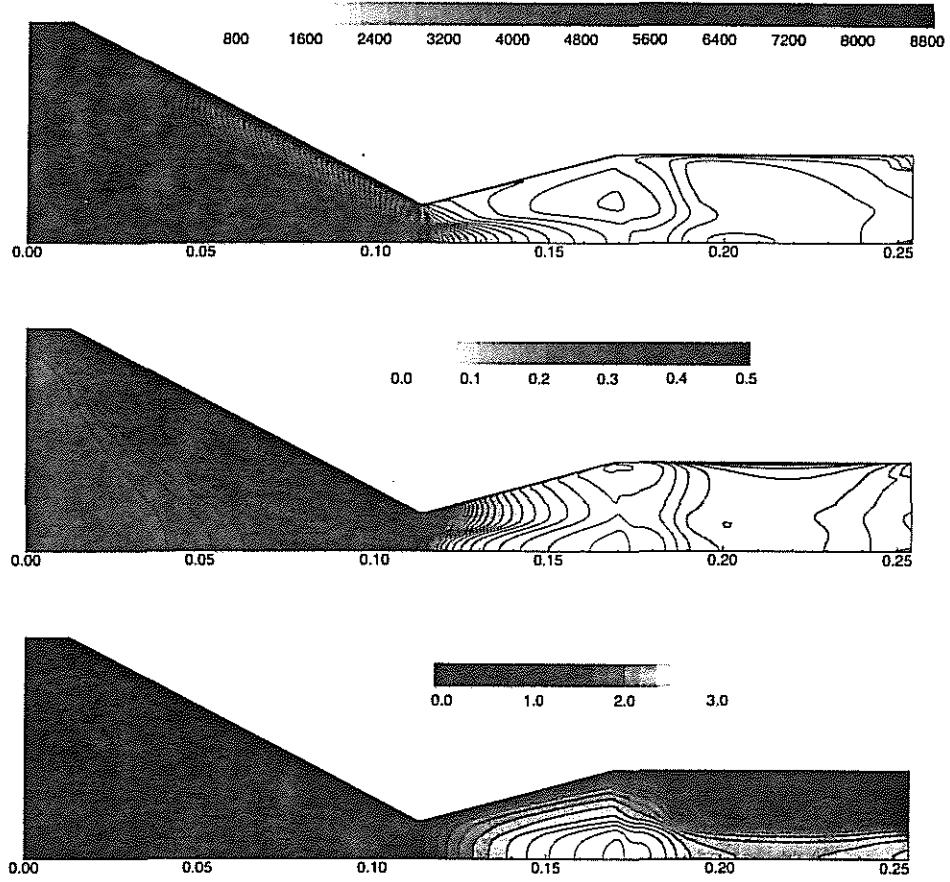


Figure 2. Gas temperature (top), density (middle), and Mach number (bottom) distributions.

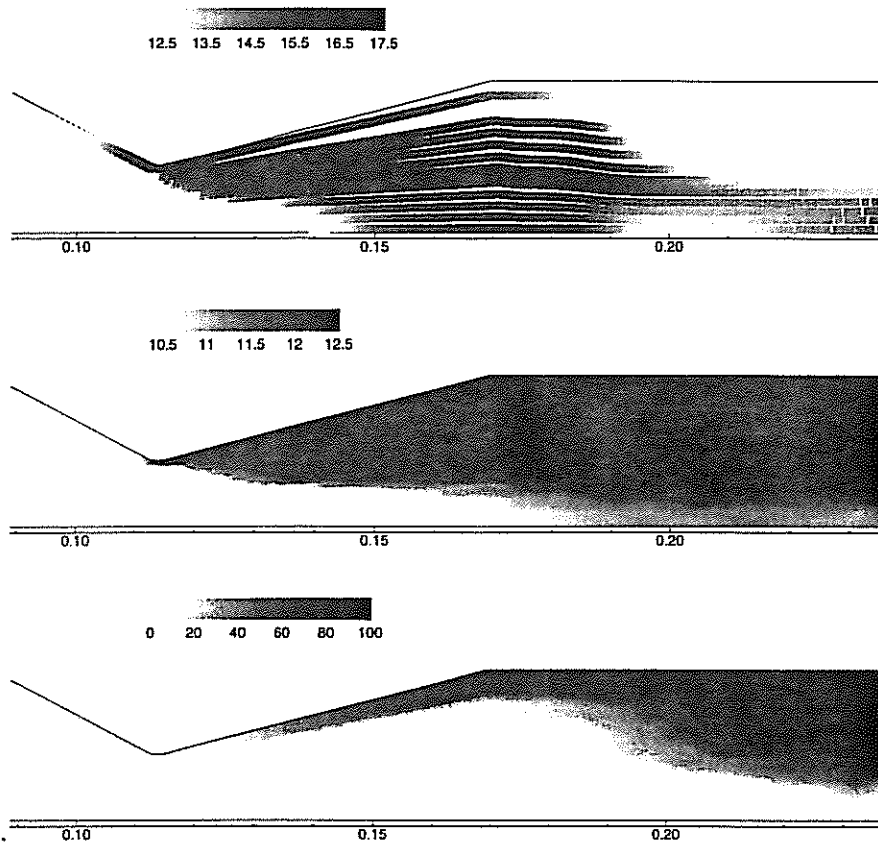


Figure 3. Log nucleation rate [particles/cm<sup>3</sup>·s] (top), log particle density [particles/cm<sup>3</sup>] (middle), and percentage of vapor condensed [%] (bottom) distributions.

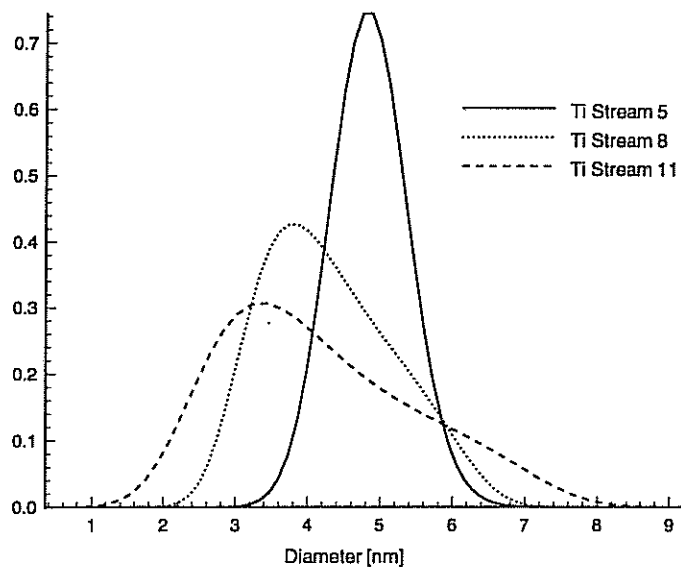


Figure 4. Normalized particle size distribution on different streamlines.

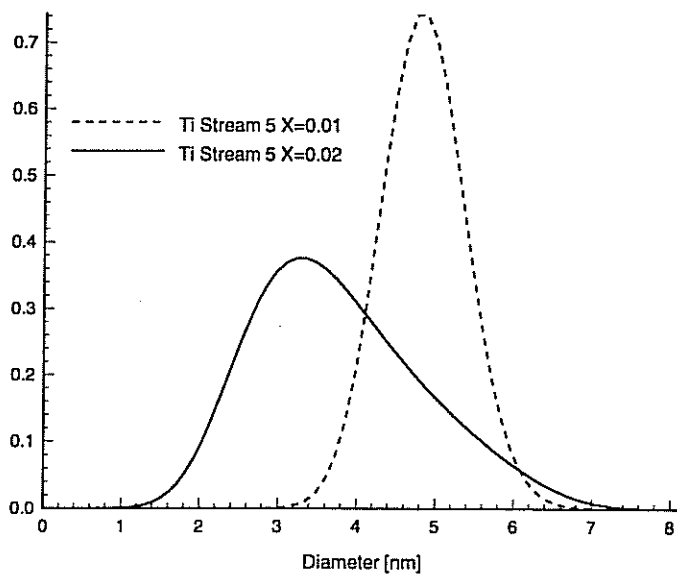


Figure 5. Normalized particles size distribution for different inlet flow titanium concentrations.

phenomena occurring in the plasma quench reactors (PQR's) can be simulated. It is emphasized here that the simulations presented are for a model problem and were not configured to represent the details of any particular PQR system. This technique awaits further verification with experimental data, but has provided very useful insight into the design and operation of such systems.

#### Acknowledgement

This work was supported through the Long-Term Research Initiative in Chemical Sciences and Laboratory Directed Research and Development under DOE Idaho Operations Office Contract DE-AC07-76ID01570 and DE-AC07-94ID13223, and NASA Agreement W-18429 under DOE Chicago Operations Office Contract DE-AC02-76CH00016.

#### References

1. S. V. Joshi, et al., Plasma Chem. Plasma Process., 10 (1990), 339; H. Ageorges, et al., ibid., 13 (1993), 613.
2. Randall A. LaViolette, Ray A. Berry, and Robert McGraw, "Homogeneous Nucleation of Metals in a Plasma-Quench Reactor," submitted for publication to Plasma Chem. Plasma Process.
3. H. C. Yee, R. F. Warming, and A. Harten, J. Comput. Phys., 57 (1985), 327.
4. P. L. Roe, J. Comput. Phys., 43 (1981), 357.
5. S. Yoon and A. Jamison, AIAA Paper 87-0600, (1987); S. T. Imlay, D. W. Roberts, and M. Soetrisno, AIAA Paper 91-2153, (1991).
6. "INCA: 3D Multi-Zone Navier-Stokes Flow Analysis with Finite-Rate Chemistry," (Report, Amtec Engineering, Inc., Bellevue, WA).
7. R. McGraw and J. H. Saunders, Aerosol Sci. Tech., 3 (1984), 367.
8. W. G. Courtney, J. Chem. Phys., 36 (1962), 2009.
9. H. M. Hulbert and S. Katz, Chem. Eng. Sci., 19 (1964), 555.
10. R. McGraw, J. Chem. Phys., 75 (1980), 5514.
11. H. Reiss, J. L. Katz, and E. R. Cohen, J. Chem. Phys., 48 (1968), 5553.
12. J. Einbu, IEEE Trans. Info. Theory, IT-23 (6) (1977), 772.
13. W. H. Press, et al., Numerical Recipes in Fortran, Second Edition (New York, NY: Cambridge University Press, 1992).
14. B. Baldwin and H. Lomax, AIAA Paper 78-257, (1978).